

60th ANNIVERSARY OF THE JOINT INSTITUTE FOR NUCLEAR RESEARCH (JINR) PACS numbers: 37.10.Ty, 41.75.Fr, 52.27.Ep, 52.27.Jt

Traps for storing charged particles and antiparticles in high-precision experiments

M K Eseev, I N Meshkov

DOI: 10.3367/UFNe.0186.201603f.0321

Contents

Abstract. The storage and confinement of charged particles and antiparticles (electrons, positrons, ions) in open traps and storage rings of various designs are considered. Experiments on positron storage in the Penning – Malmberg – Surko trap in the Low-Energy Particle Toroidal Accumulator (LEPTA) are described in detail.

Keywords: Paul trap, Penning – Malmberg – Surko trap, electrons, ions, positrons, antihydrogen, positronium, storage, rotating electric field

1. Introduction

Traps for charged particles can accumulate and confine charged particles for long periods of time. These devices are being developed and used for three purposes:

— to perform experiments on ultimate-precision measurements of the properties of particles and various nuclear, atomic, and molecular objects formed by them;

— to form dense hot plasma of hydrogen isotopes in thermonuclear generators;

— to play the role of an auxiliary unit in various experimental systems in order to store, separate, cool, and compress charged particle bunches before their injection into the elements of other systems for further experiments.

Such devices are in high demand in atomic and nuclear physics, accelerator physics, mass spectrometry, and plasma setups.

There are various designs for the traps, but in all cases the charged particles are trapped using electric and/or magnetic fields. Hence, there are general laws for charged particle motion in these traps.

This paper describes traps of the first and partially of the third type. Interest in these traps surged in 1995 after the first successful experiments by the W Oelert group on the synthesis of 11 antihydrogen atoms in the Low Energy Antiproton Ring (LEAR) at CERN [1]. Fast antihydrogen atoms (with the antiproton energy of 1.2 eV) were generated in this experiment when an antiproton captured a positron from the positron–electron pair that was produced during the interaction of that antiproton with the nucleus of a xenon atom (gas target). The cross section of this process was estimated as 6×10^{-33} cm^2 (Fig. 1).

The experiment was successful: 11 antihydrogen atoms were obtained (the noise level was 2 ± 1 atoms). This was proof of the antihydrogen ‘existence theorem’. However, this experiment could not be used to perform any kind of high-precision spectroscopy of antihydrogen or to verify the CPT theorem (which was one of the main motivations for antihydrogen production). Shortly after, two new projects were started at CERN: the Antihydrogen Apparatus (ATHENA), which was later transformed into the Antihydrogen Laser Physics Apparatus (ALPHA), and the Antihydrogen Trap (ATRAP), based on accumulation of antiprotons and protons in traps and their further recombination, followed by the formation of antihydrogen atoms. At the end of 2011, the ALPHA group demonstrated the possibility of

M K Eseev Joint Institute for Nuclear Research,
ul. Joliot-Curie 6, 141980 Dubna, Moscow region, Russian Federation;
Lomonosov Northern (Arctic) Federal University,
nab. Severnaya Dvina 17, 163002 Arkhangelsk, Russian Federation
Tel. +7 (8182) 68 31 84
E-mail: m.eseev@narfu.ru
I N Meshkov Joint Institute for Nuclear Research,
ul. Joliot-Curie 6, 141980 Dubna, Moscow region, Russian Federation
Tel. +7 (496) 216 51 93
E-mail: meshkov@jinr.ru

Received 8 July 2015, revised 7 November 2015
Uspekhi Fizicheskikh Nauk **186** (3) 321 – 335 (2016)
DOI: 10.3367/UFNr.0186.201603f.0321
Translated by A L Chekhov; edited by A M Semikhatov

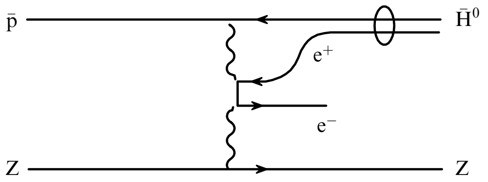

Figure 1. Feynman diagram for the process of antihydrogen atom formation during the antiproton interaction with the electromagnetic field of a heavy nucleus.

holding an antihydrogen atom in a magnetic trap for 17 minutes [2]. This meant that antihydrogen atom spectroscopy is possible in principle [3].

Meanwhile, at CERN, the Atomic Spectroscopy and Collisions Using Slow Antiprotons (ASACUSA) group was developing a method for 'in-flight' spectroscopy of the antihydrogen atom flux [4]. The Gravitational Behaviour of Antihydrogen at Rest (GBAR) and Antihydrogen Experiment: Gravity, Interferometry, Spectroscopy (AEGIS) projects are aimed to study the influence of gravitation on antimatter particles (antihydrogen atoms) as they fall in Earth's gravitational field.

The GBAR group [5] generates a bunch of positronium atoms (electromagnetically coupled electrons and positrons) using the interaction of an intensive positron flux with a hydrogen target and bombards this bunch with antiprotons. Antiprotons recombine with positronium atoms and form 'anti-ions' — positively charged antihydrogen ions $\bar{H}^+$. These anti-ions are thermalized in the magnetic field by Be^+ ions and ionized by laser radiation. After that, they freely fall on the walls of the vacuum chamber. The detector registers the spatial distribution of the annihilation regions of antiprotons, which allows measuring their shift and determining the possible 'antigravitation' effect (or its upper bounds). In the AEGIS project [6], antiprotons are injected into a positronium cloud, which is excited by the laser radiation. After the recombination, a hydrogen atom flux forms, and the gravitational shift of this flux is measured while passing the detector. Both these experiments are at the stage of setting-up procedures, which should be completed in 2017, when the Extra-Low Energy Antiproton (ELENA) storage ring will start operating.

The success of CERN experiments in the field of antihydrogen physics [7] would be impossible without the development of particle accumulation and confinement technologies (for positrons, antiprotons, and antihydrogen) in electromagnetic traps.

Experiments with positronium atoms are also of great interest. These exotic 'atoms' are traditional objects of research in particle physics [8]. The most famous work in this field of physics has been done in the Positron Research Group under the direction of K Surko at the University of California, San Diego [9]. Surko's group investigates the processes of positron interaction with atoms and molecules [10]. This group is building the biggest trap in the world for low-energy positrons, which can confine more than 10^{12} particles.

Another research center for positron and positronium physics is the laboratory at the University of California, Riverside, where in 2007 Cassidy and Mills succeeded in producing molecular positronium [11] and positroniums in Rydberg states with a long lifetime [12] and started measurements of optical transitions in molecular positroniums [13]. These experiments were performed using the Penning–Malmberg–Surko (PMS) trap, discussed in Section 4.

'Trapping' experiments in the antiproton and ion physics are currently being planned in Germany at the Facility for Antiproton and Ion Research (FAIR). Within this project, a variety of Facilities for Low-energy Antiproton and Ion Research (FLAIR) will be built, where, in particular, experiments on production and investigation of antihydrogen will be carried out. This will be the follow-up of experiments at CERN on antihydrogen interatomic transitions and on the influence of gravity on antimatter, which are being conducted or prepared at the moment.

In all the experiments mentioned above, a significant role is played by traps for the charged particles that are parts of the produced 'exotic' atoms. Only by keeping antiparticles from annihilation with matter can antimatter beams be accumulated and maintained for further experiments.

In modern experiments, the traps are used not only for exotic atoms and antimatter. In Section 2, we present examples of electromagnetic trap applications in various fields of atomic and nuclear physics, plasma physics, and so on.

The present review provides a short history of the discovery and development of 'trapping' devices in physical experiments and describes the most common types of traps and some of their applications. We pay special attention to the so-called Penning–Malmberg trap and its modern modifications and also discuss the results of theoretical and experimental investigations of the particle accumulation dynamics (for electrons and positrons) in this trap.

2. History of the development of traps and storage devices and their applications

Electromagnetic traps allow confining and investigating single particles and groups (bunches) of particles [14, 15]. In the first case, the trapping allows performing high-precision measurements of particle properties; in the second case, intensive and controllable beams of accumulated particles can be obtained. Electromagnetic traps can confine not only charged elementary particles or ions but also neutral atoms if they have a nonzero dipole or magnetic moment. In this review, we limit our considerations to charged particle traps. In Sections 3 and 4, we present detailed descriptions of the construction and operating principles of such traps. In this section, we focus on a retrospective and on the main stages of development and application of traps.

The applications of traps are similar to those of storage rings/accelerators, but they differ in design and particle dynamics. Storage devices can confine charged particle bunches with significantly higher intensity (see Section 5), which can then be injected into accelerators or used in experiments on synchrotron (magneto-brehmsstrahlung) radiation. Traps and storage devices also differ in the methods of particle cooling. Storage facilities use electron and stochastic cooling, while electromagnetic traps employ buffer gas and laser cooling. Radiative cooling can also be used in traps and storage devices for electrons or positrons.

The use of traps and storage rings in experimental physics started almost simultaneously in the 1950s. It began with ideas of closed-type traps to hold ions in order to perform controlled thermonuclear synthesis — 'tokamak' (abbreviation from the Russian "Toroidal camera with magnetic coils,'' which became a common noun) (1950), made by Sakharov and Tamm [16], and the 'stellarator' (from 'stellar'), made by Spitzer [17]. The first open-type magnetic trap ('probkotron') was independently suggested in 1953–1954 by Budker [18] and by Post [19].

At the same time, scientists started working on long-term confinement and cooling of a relatively small number of charged and neutral particles. Pierce was the first to propose a design for this type of trap in 1949 [20]. But only 10 years later, Dehmelt managed to make a working setup [21, 22], where a single electron could be held for a long time [23]. He named this trap after Penning, who was the first to suggest using a longitudinal magnetic field in order to hold the plasma formed in an electric discharge [24]. The first radio-frequency Paul ion trap was made in 1953 [25]. Paul and Dehmelt received a Nobel Prize in 1989 for their work on traps and experiments on confinement and controlling the states of ions and electrons [26, 27].

In the late 1950s, two groups started their 'competition' in the development of the first storage rings with counter-propagating electron beams. One of them was based at the Stanford Linear Accelerator Center (SLAC) (USA) and the other at the Institute of Nuclear Physics of the USSR Academy of Sciences (INP) (Novosibirsk). This was the beginning of the 'collider era' (see review [28]). After 65 years of development, storage ring/colliders play a leading role in high-energy physics. The particle energy in these devices has increased from modest values of several hundred MeV to the TeV range. However, there are still many interesting problems in the low-energy range, where particles with the lowest possible energies are in demand. We discuss this in Section 3.4.

The idea of traps that could hold neutral particles with a magnetic moment appeared in 1960. The first suggestion was made by Vladimirskii, who formulated the operation principle of traps with a magnetic field minimum [29]. Shortly after, the M S Ioffe group found a solution to the technical design of such a trap [30]. However, Pritchard was the first to realize these ideas [31]. The device for holding neutral particles with a magnetic moment was named the Ioffe–Pritchard trap.

We note that Ioffe–Pritchard traps are also interesting for charged particle trapping, and there were attempts to build such traps for thermonuclear applications. Neutral particle traps are often similar to charged particle traps. Neutral particles that have negative polarizability are trapped using a special electrostatic field configuration and the Stark effect. These are highly excited (Rydberg) atoms and some molecules. Neutral particles with a nonzero magnetic moment can be confined in traps like the probkotron due to the specific distribution of magnetic fields [32]. Success in the field of laser cooling and trapping of atoms with light [33] allowed the design of a magneto-optical trap for atoms. The head of the Stanford University group, S Chu, received the Nobel Prize in 1997 for achievements in this field [34]. Atom traps and various cooling methods allowed obtaining the Bose–Einstein condensate of atoms in 1995, and in 2001, Cornell, Ketterle, and Wieman received the Nobel Prize for this achievement [35]. We also note the success in the field of quantum computer development. In 2012, the Nobel Prize was awarded to Wineland and Haroche ''for ground-breaking experimental methods that enable measuring and manipulation of individual quantum systems'' [36]. Laser cooling of ions in quadrupole traps helped to demonstrate the fundamental possibility of controlling quantum systems, which opens up possibilities to perform quantum computations.

In 1978, Dehmelt's group suggested [37] accumulating positrons — antimatter particles — in a trap using the magnetron drift, and realized it in 1981 [38]. The results of this work simultaneously attracted attention to the problems of the positron and positronium physics. This started the independent development of the Penning trap, which in its modern modification led to the success mentioned in the Introduction.

Penning and Paul traps are used in nuclear physics for accumulation of ions, their separation [39], and high-precision mass spectrometry. Typically, gas-filled Paul traps are used with four cylindrical rods as electrodes, which form a transverse quadrupole electrostatic field. These traps are used either for fast cooling of ion beams in experiments on laser spectroscopy or as the injector for Penning traps. Penning traps allow separating ion beams and performing precise measurements of ion masses by sideband cooling [27]. In one of the Penning trap modifications — the Electron Beam Ion Trap (EBIT) — an electron beam is injected into the storage region in order to create ions via the ionization process [40].

There are a number of well-known experimental setups with traps in the field of nuclear physics, which include the ISOLTRAP, WITCHTRAP and REXTRAP (Radioactive Experimental Trap) of the Isotope Mass Separator On-line Detector (ISOLDE) complex at CERN, Canadian Penning Trap (CPT) at the Argonne National Laboratory, USA, SHIPTRAP at the GSI Helmholtz Centre for Heavy Ion Research (Darmstadt, Germany), JYFLTRAP at the University of Jyv'skyl', Finland, Low-Energy Beam and Ion Trap (LEBIT) at Michigan State University, USA, TRIUMF's Ion Trap for Atomic and Nuclear Science (TITAN) at the TRIUMF research center (Vancouver, Canada), LPC trap (Laboratoire de Physique Corpusculaire) at the GANIL laboratory (Grand Accélérator National d'Ions Lourds), France, Training Research Isotope General Atomic Trap (TRIGA-TRAP) at the Research Reactor Laboratory (Mainz, Germany), Florida State University trap (FSU trap) (Florida, USA), and Tritium–Helium trap (THe trap) at the Max-Planck Institute (Heidelberg, Germany).

An excellent example is the ISOLDE complex, which was built for experiments on radioactive nuclei and ions. Part of this setup is a set of Penning traps. Penning traps were used to perform precise measurements of radioactive ion masses in the ISOLTRAP experiment [41]. The first trap with a field of 4.7 T created by a superconducting coil accumulates and selects ions, which are preliminarily cooled in other parts of the setup. The second trap, with a magnetic field of 6 T, is used to perform precise measurements of the mass of a small number of ions by mass-spectrometry methods. Absolute values of mass are determined using ^{12}C reference nuclei, which results in a measurement accuracy $\Delta M/M < 10^{-8}$. This method was used to measure the masses of radioactive isotopes with half-lives up to 60 ms. The experiment resulted in new and updated data for more than 400 radioactive isotopes. Similar experiments have been performed over many years at the GSI Experimental Storage Ring (ESR) [42] with electron cooling. At the ISOLDE complex, Paul traps are also used for ion separation.

In Section 3, we describe the operation principles of some traps used in modern experiments with positrons and positronium.

3. Storage and confinement of charged plasma in traps and storage devices

3.1 Paul trap

The classic radio frequency Paul trap [25, 26] consists of three electrodes, which are hyperboloids of revolution with a common axis (Fig. 2). In the case of positrons, the front cap electrodes have a positive potential and the middle electrode has a negative potential. This creates an electrostatic field, which holds particles close to the center of the trap. The voltage applied to the electrodes has a DC part U_0 and an AC part with an amplitude V_0 and frequency Ω. The polarities are chosen in a particular way to form a quadrupole field in the trapping region with the potential

$$\Phi(x,y,z) = \frac{\big(U_0 + V(t)\big)(x^2+y^2-2z^2)}{2r_0^2}\,, \qquad (1)$$

where r_0 is the inner radius of the middle electrode in the xy plane, $r_0^2 = 2z_0^2$, z_0 is the distance between front electrodes along the z axis, and U_0 and $V(t) = V_0 \cos(\Omega t)$ are the DC and AC voltages applied to the electrodes. The origin of the coordinate system is chosen in (1) at the center of the trap. Here and hereafter, we use the Gaussian system of units. We specify those cases where the SI units are used.

If the AC voltage is turned off ($V_0 = 0$) and the polarity is the same as in Fig. 2, the potential $\Phi(x,y,z)$ creates a stable equilibrium position for a positively charged particle in the middle plane of the trap ($r = 0$) and an unstable one in the direction perpendicular to the z axis. In this case, the particle 'falls down' from the unstable equilibrium position to the inner wall of the middle electrode. If the AC voltage $V(t)$ is turned on, the particle motion can be described by the Mathieu equations (see [26]), which have a stable solution for a specific set of parameters U_0, V_0, and Ω (Mathieu equation stability zone). In this case, a stable equilibrium position exists at the center of the trap, $x = y = z = 0$. Optimal values of the mentioned parameters depend on the ion type (its charge and mass). Therefore, the Paul trap can be used as a mass analyzer.

Besides the design described above, there are other types of Paul traps. In particular, a trap without cap electrodes, the so-called linear trap, which has four hyperboloid electrodes extending along the common axis (in the simplest case, cylindrical rods), is used in time-of-flight mass spectrometers. Such a trap analyzer was used in the first maser made by Prokhorov and Basov (1964 Nobel Prize). This trap allows cooling single ions to very low temperatures and observing crystallization of small groups of ions [43].

The Paul trap, despite its obvious advantage — construction simplicity — has one significant disadvantage: the size of its particle storage region is limited, which does not allow storing a large number of particles. This is one of the limitations for the Paul trap applications.

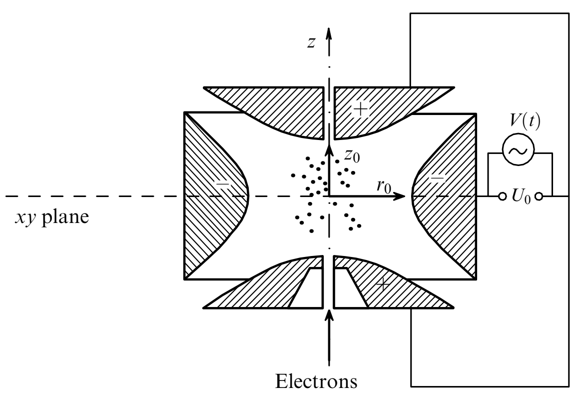

Figure 2. Schematic of a Paul trap (cross section) [26].

3.2 Penning trap

By turning off the AC voltage in the Paul trap and adding a magnetic field parallel to its axis, we arrive at the design of the Penning trap (Fig. 3), which was made by Dehmelt [27]. Superposition of the axially symmetric electric **E** and magnetic **B** fields of the trap determines a quite complicated motion trajectory for particles in the trap — longitudinal bounce-oscillations with a frequency f_{bounce} and cyclic motion in the plane transverse to the axis (Fig. 4). The latter is a combination of a fast cyclotron rotation with a frequency f_c and a relatively slow 'magnetron' rotation in the crossed fields $\mathbf{E}_r$ and **B** with a frequency f_{magn}. For a particle with the charge eZ and mass m in an electric field with potential (1) and under the condition of a strong field ($f_c \gg f_{\text{magn}}$), there

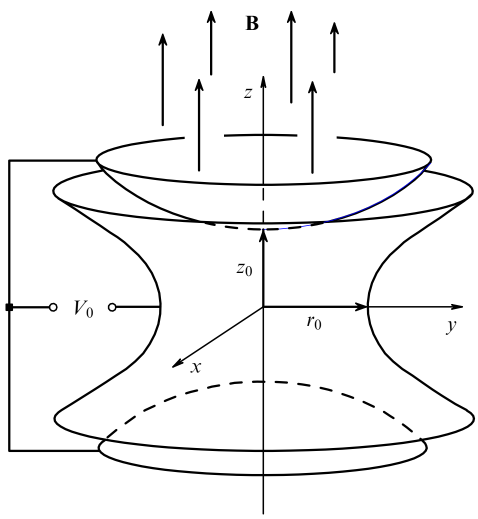

Figure 3. Schematic of a Penning trap.

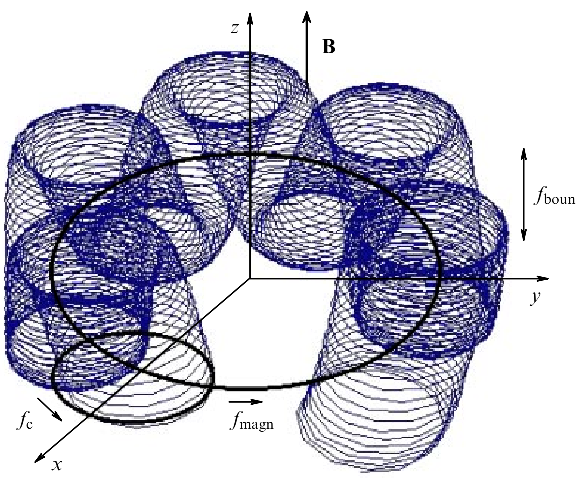

Figure 4. Particle trajectory in a Penning trap.

frequencies can be written as

$$f_{\text{bounce}} = \frac{1}{\pi}\sqrt{\frac{eZV_0}{m(r_0^2 + 2z_0^2)}}\,,$$
$$f_{\text{c}} = \frac{eZB}{2\pi mc}\,,$$
$$f_{\text{magn}} = \frac{cV_0}{\pi B(r_0^2 + 2z_0^2)}\,. \qquad (2)$$

The frequencies in (2) depend on the values of the fields and the trap geometry. Such motion is typical for magnetrons, which explains the term 'magnetron rotation'. In comparison with the Paul trap, this trap has a much stronger 'focusing' of particles in the transverse direction, which allows storing high-intensity particle bunches (see Section 5).

3.3 Penning–Malmberg trap

The Penning–Malmberg trap [44] is a modification of the Penning trap where the electrodes — hyperboloids of revolution — are replaced with segments of round cylindrical tubes (Fig. 5). A static potential is applied to the electrodes in such way that a trapping potential is created along the axis. This holds the particles in the longitudinal direction. A static longitudinal magnetic field **B** keeps the particles from falling on the electrode walls. A large space between the cylinders and the ability to create a high potential difference allows a much larger number of particles to be confined than in the traps described in Sections 3.1 and 3.2.

The distribution of the potential inside the cylinders is described by the expression [45, 46]

$$\Phi(r,z) = 2V_0 \sum_i^{\infty} \frac{J_0(\mu_i r/r_0)\cosh(\mu_i z/r_0)}{\mu_i J_1(\mu_i)\cosh(\mu_i z_0/r_0)}\,, \qquad (3)$$

where $r = \sqrt{x^2+y^2}$, J_0 and J_1 are the Bessel functions of the first kind of the first and second order, and μ_i are the roots of these functions.

Close to the axis and the center of the trap ($\mu_i r \ll 1$ and $\mu_i z \ll 1$), solution (3) can be simplified and expressed in a form close to the electrostatic field of an axially symmetric quadrupole:

$$\Phi(r,z) \approx 2V_0 \sum_i^{\infty} \frac{1}{\mu_i J_1(\mu_i)\cosh(\mu_i z_0/r_0)} - V_0\,\frac{r^2 - 2z^2}{2r_0^2} \sum_i^{\infty} \frac{\mu_i}{J_1(\mu_i)\cosh(\mu_i z_0/r_0)}\,. \qquad (4)$$

According to (4), the motion of particles in this trap can be described with good accuracy in the same way as in the Penning trap by separating it into longitudinal oscillations and cyclic rotation.

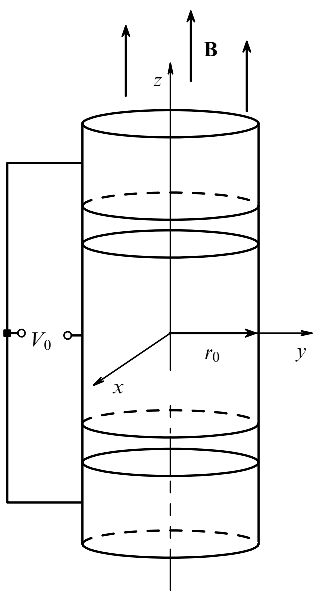

Figure 5. Schematic of the Penning–Malmberg trap.

3.4 Storage rings: traps for charged particles

As was mentioned in Section 2, charged particles are stored in circular 'magnetic ringroads'. The transverse deflecting and focusing magnetic fields are used in order to confine (focus) the high-energy particles inside them. In storage rings with 'soft' focusing, these functions are combined in dipole magnets with an inhomogeneous field that decreases as r^{-n} with the main ring radius. A stability condition for particle motion along the ring defines the exponent value $0 < n < 1$. In hard-focusing storage rings, the functions are separated: deflecting is controlled by magnets with a homogeneous field and the focusing (particle confinement) by magnets with a quadrupole field.

For low-energy particles, a much more efficient way is to store and confine them in the longitudinal magnetic field of a toroidal solenoid (tokamak) or a closed solenoid in the form of a racetrack (stellarator). The second option is realized in the LEPTA (Low Energy Particle Toroidal Accumulator) storage ring designed and constructed at the Joined Institute for Nuclear Research (JINR) [49].

The main application of the LEPTA facility is the generation of high-intensity positronium flux for performing high-precision measurements of positronium characteristics and searching for 'new physics' in positronium decay (annihilation). The positronium flux is produced by recombination of positrons circulating in the LEPTA storage ring with the same mean velocity (by the modulus and direction) as that of positrons. The positrons are simultaneously cooled by electrons. This results in the formation of a narrow flux of positronium atoms.

The storage ring (Fig. 6) consists of two toroidal and two rectilinear solenoids, connected into a racetrack-type magnetic track. On one of two straight sections, the solenoids

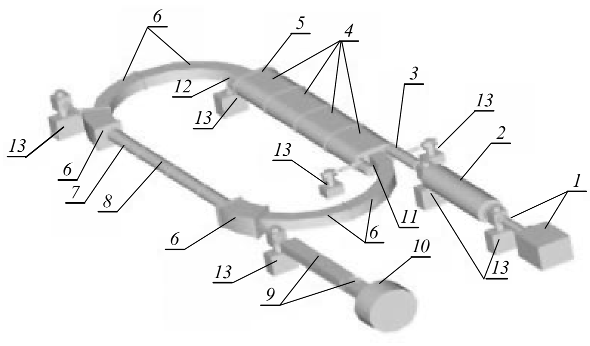

Figure 6. Schematic of the LEPTA storage ring: *1* — positron source, *2* — positron trap, *3* — positron injection section, *4* — septum solenoids, *5* — kicker (placed in the septum coil), *6* — toroidal solenoids, *7* — straight solenoid and quadrupole coil, *8* — electron cooling section, rectilinear coil, *9* — analyzing magnet, *10* — detector, *11* — electron gun, *12* — electron collector, *13* — vacuum pumps.

have the form of a round cylinder, and on the other they have the form of a cylinder with an elliptic cross section. These are the so-called septum solenoids. The source of electrons (an electron gun), their collector, and the positron injector are situated inside additional solenoids. All the solenoids are surrounded by a common magnetic screen. A vacuum chamber is situated inside the solenoids. A single-turn injection of positrons is performed by an electric kicker.

Positrons are transported from injector *1*, *2* (see Fig. 6) to septum solenoid *4* by channel *3*. While passing through this solenoid, the positrons are forced by the additional transverse magnetic field to shift to the left in the horizontal plane, and they exit the septum exactly above the equilibrium orbit. Kicker *5* is located after the septum solenoid, and it shifts the positrons down in the vertical plane, bringing them on an equilibrium orbit. The kicker turns off as the positrons fill the whole circumference of the ring. After the kicker, the positrons enter the first arc, which consists of one long and one short toroidal solenoid *6*. Besides the longitudinal magnetic field, a vertical magnetic field is created in the arc. The latter is needed to compensate the centrifugal gradient drift of positrons in the toroidal solenoid.

At the beginning of straight section *7*, *8*, the positrons overlap with electrons (see below) and are accompanied by them before entering the second arc. This stage is where the electrons and positrons recombine and produce positronium. Electrically neutral long-lived atoms of orthopositronium (o-Ps) are directed to experimental channel *9* with detector *10*. The short-lived component, parapositronium (p-Ps), decays in the channel. After passing through the cooling section, positrons first enter the second arc *6* and then septum solenoid *4* and pass through it to the equilibrium trajectory channel.

The electron beam is injected by electron gun *11*, situated at the entrance to the septum solenoid on the left-hand side and lower than the positron equilibrium trajectory. While passing through the septum coil, electrons are influenced by the transverse magnetic field of the septum and shift to the right in the horizontal plane towards the positron equilibrium trajectory and then enter the kicker. At the beginning of the electron injection, the positron beam injection finishes and the kicker is turned off. Therefore, the electron beam passes through the kicker unshifted. At the entrance to the first arc, the electrons appear lower than the positron beam. Because the drift direction in the toroidal solenoid is determined by the sign of the particle charge and the additional vertical magnetic field compensates the positron drift, the electrons experience a drift in the opposite direction and their shift doubles.

The parameters of the setup are such that after passing the first arc, the electrons are lifted towards the positron trajectory, and the beams overlap at the entrance to the straight section. After passing through the straight section in the second arc, the beams separate from each other due to the electron drift — electrons rise, enter the exit channel of the septum solenoid, and head towards the collector. It has a potential that is close to the gun cathode potential (electron energy recovery regime). This significantly lowers the level of resistance losses in the gun source and the collector heating.

Focusing (confinement) of charged particles in the LEPTA is realized by the longitudinal magnetic field, which is present in every part of the circulating beam orbit. To ensure the stability of the particle motion along the equilibrium orbit, an additional spiral quadrupole field is used together with the longitudinal magnetic field. This additional field is produced by a special winding (similarly to the case of stellarators).

A feature of the storage device with a longitudinal magnetic field is that the electron cooling of circulating positron decreases their temperature but does not change the transverse size of the beam. Each positron is cooled while being ‘attached’ to its own magnetic field line, and therefore the spread of positron velocities is determined by the difference of the field potential of the electron beam's space charge on the size of the positron beam. This potential difference depends on the degree of natural neutralization of the electron beam, which is in turn dependent on the residual gas pressure and the vacuum chamber geometry (the variation of the transverse size of the chamber along the positron orbit).

The positron injector at the LEPTA has two main elements: a positron source and a trap for positron accumulation. The cryogenic positron source was developed at the Joint Institute for Nuclear Research (JINR) and is based on a β^+-active emitter, the ^{22}Na isotope, which was made at the iThemba research institution, Laboratory for Accelerator-Based Sciences (LABS), Republic of South Africa. The positrons are slowed down in a layer of solid neon, which is frozen at the temperature of 5 K on top of a titan foil 5 μm wide that covers the output window of the emitter, and the low-energy components of the spectrum are separated in the magnetic field. The full spectral width of the positrons emitted from the ^{22}Na isotope is around 500 keV, and it is possible to separate approximately 1% of the positron flux with an energy of the order of several electron volts with the FWHM around 1.5 eV (Fig. 7).

The trap in the LEPTA has the same design and operation principles as the Penning–Malmberg–Surko trap, which is described in Section 4.

The first physical problem that was planned to be solved at the LEPTA was to obtain long-time circulation of particles in it. There were several attempts to create similar storage devices before, but none of them resulted in a long enough circulation time [50]. The LEPTA facility achieved a significant progress in solving this problem. After correcting

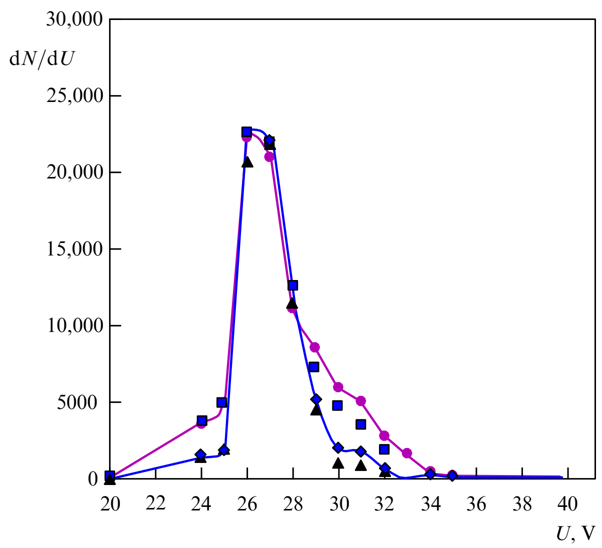

Figure 7. Differential spectrum of positrons in the source output for the moderator thickness of 75 μm (circles and squares) and 95 μm (triangles and diamonds).

Table 1. Design parameters of the LEPTA.

Parameter	Value
Circumference, m	17.2
Positron energy, keV	4 – 10
Period of revolution, ns	500 – 300
Longitudinal magnetic field, G	400 – 600
Larger radius of toroids, m	1.45
Helical quadrupole field gradient, G cm^{-1}	10
Positron beam radius, cm	0.5
Number of circulating positrons	10^8
Residual gas pressure, Torr	10^{-10}
Electron cooling system	
Cooling section length, m	4
Electron beam current, A	0.5
Electron beam radius, cm	1
Orthopositronium flux parameters	
Rate, number of atoms per s	10^4
Angular spread, mrad	1.0
Energy spread, $\Delta v/v$	10^{-3}

the magnetic field and improving the vacuum, the lifetime of the beam in the accumulator increased to 0.17 s [49, 51].

The second problem is the electron cooling of positrons and production of positronium. If this problem is solved, many unique experiments will be performed with directed positronium fluxes [52, 53]; this will be possible as the design values of the LEPTA parameters are reached (Table 1).

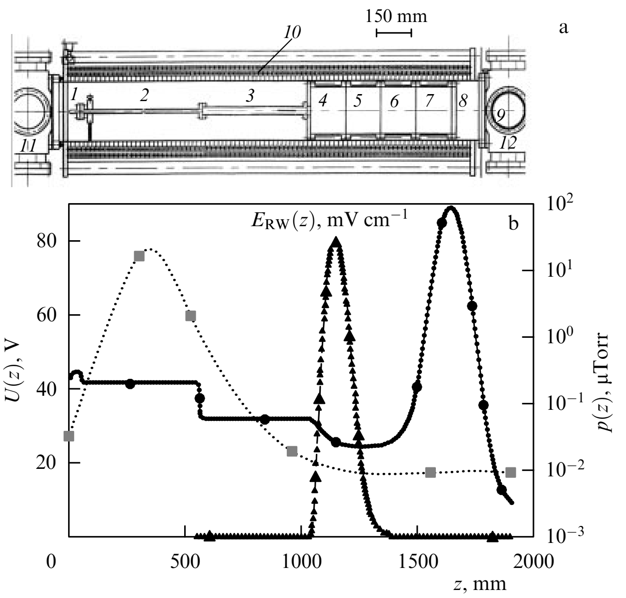

Figure 8. (a) Schematic of the PMS trap in the LEPTA setup. *1–8* — electrodes (split electrode 4 is used to create the RW field), *9* — collector and a scintillation counter, *10* — coil, *11*, *12* — turbomolecular and cryogenic vacuum pumps. (b) Distribution of the electric field potential of the electrodes $U(z)$ (circles — numerical modeling), the RW field $E_{\rm RW}(z)$ (triangles — numerical modeling), and the buffer gas pressure $p(z)$ (squares — calculation based on the pressure measurement at the input and output of the trap) over the chamber axis in the positron accumulation regime.

4. Penning–Malmberg–Surko trap with a rotating electric field

4.1 Design and operation principle of the Penning–Malmberg–Surko trap

One of the main problems in trapping technologies is particle injection. It is especially important when storing particles from low-intensity sources. For example, in traps of all the types discussed in Sections 3.1–3.3, multiple repetitions of injection are very difficult due to size limitations and design features. Notably, it is almost impossible when using radioactive positron sources, which produce a continuous flux with an intensity that fluctuates over time. The situation is simpler when one short and intensive particle bunch formed in accelerators or storage rings can be injected. An important solution was found by Surko, who suggested a positron storage scheme in the Penning–Malmberg trap using a buffer gas with a pressure gradient along the length of the trap [54]. This modified trap was named the Penning–Malmberg–Surko (PMS) trap.

Later, storage efficiency was improved again by using a rotating electric field in order to increase the charged plasma lifetime. This 'rotating wall' (RW) effect was observed in experiments on the accumulation of plasma bunch Mg^+ ions [55]. After that, similar results were obtained for both electron and positron plasmas [56, 57].

The rotating field method is used for antihydrogen generation in the ATHENA/ALPHA project [58]. The success of using this method allowed studying properties of antimatter and exotic atomic–molecular systems [3, 9, 13, 59]. The accumulation is controlled by the frequency and direction of the field rotation in the plane perpendicular to the trap axis. The accumulation efficiency resonantly depends on the RW-field parameters. The mechanism of rotating field interaction with the bunch does not yet have a clear explanation, which is noted in [60, 61].

In our experiments at the LEPTA facility, we used a PMS trap with a rotating electric field. The positrons were first accumulated in it and then injected into the storage ring for further production of positronium [48, 49]. The aim of our research on particle accumulation in a trap was to find optimal methods and accumulation parameters and to experimentally verify possible mechanisms for particle bunch compression in a rotating electric field.

The trap used in the LEPTA facility [62] has a standard PMS geometry, shown in Fig. 8. The electrode line is placed in a cylindrical vacuum chamber, which is located inside a solenoid that creates a coaxial longitudinal magnetic field. Vacuum pumps are situated at both ends of the chamber. They are needed to remove the residual gas, which shortens the particle lifetime in the trap, and to create a buffer gas pressure gradient (see Fig. 8). The latter is realized by a special geometry of eight cylindrical electrodes isolated from each other and having different lengths and diameters. The gas is injected through an opening in the middle of electrode *2* and is pumped out at the ends of electrodes *1* and *8*. As a result, the pressure has a specific distribution between the entrance into the trap (electrode *1*) and the accumulation region (electrodes *4–7*), as shown in Fig. 8b.

Positrons are captured by the trap and cooled via inelastic collisions with nitrogen molecules. The pressure is such that after leaving the source and passing through electrode *2*, the positron would on average experience one inelastic collision. After losing its energy in this collision, the positron cannot overcome the potential of electrode *1* and leave the trap. Subsequent inelastic collisions lead to the confinement of the positron in a potential well in region *4–7*.

Table 2. Typical values of the parameters of the particles and trap during accumulation.

Parameter	Variation range
Longitudinal magnetic field B, G	800 – 1200
Cyclotron frequency ω_c, s^{-1}	$(1.3-2.0)\times10^{10}$
Depth of potential well in the accumulation region (with respect to electrode *1*) U_0, V	15 – 20
Pressure in the accumulation region during gas puffing P, Torr	$10^{-8}-5\times10^{-6}$
RW-field amplitude, V cm^{-1}	0.5 – 2.0
RW-field rotation frequency (the sign corresponds to the rotation direction with respect to the direction of bunch magnetron rotation) f_{RW}, kHz	$0-\pm1400$
Radius of the electrodes *4–8* R_0, cm	10
Length of the electrodes in the accumulation region L_0, cm	15.0
Density of accumulated particles n, cm^{-3}	$\leqslant 10^8$
Plasma frequency ω_p, s^{-1}	$\leqslant 2\times10^8$
Transverse size of the Gaussian bunch σ_r, cm	$\sim$0.5
Length of the accumulated bunch, L, cm	12.0 – 50.0

The positron energy at the entrance to the trap and the electrode potential distribution are designed such that positrons have an energy of the order of 1 eV in the storage region (Fig. 8b). After that, the positrons lose their energy in the collisions by exciting rotational and vibrational modes of buffer gas molecules and cool down to room temperature ($\approx$ 26 meV). The accumulation process continues until the supply of positrons from the source is compensated by their annihilation with the residual gas and diffusion on the chamber walls. The distributions of the nitrogen pressure and trap potential determine the positron energy and are critical for the accumulation process efficiency. The choice of nitrogen as the buffer gas is explained by the small annihilation cross section of this gas and positrons with energies typical for this experiment.

To create an RW field in the trap, electrode *4* is designed as four isolated segments. Each segment receives a harmonic AC voltage with the same frequency and amplitude, but with a phase shift of 90° with respect to the adjacent segment. This results in electric field rotation in the plane perpendicular to the trap axis. Typical values of the variable parameters and characteristics of the accumulated particle bunch in our experiment are shown in Table 2.

4.2 Accumulation of particles in traps with a rotating field
Experiments on the RW-field influence on the particle accumulation process were performed in 2009–2015 in the PMS trap at the LEPTA for positrons and electrons. These experiments confirmed the effects observed by other scientists [55–58] and revealed new effects that had not been observed before.

Experiments with positrons were performed using the source described in Sections 3 and 4. To measure the intensity of the accumulated bunch, the positrons were extracted from the trap to collector *9* (Fig. 8a) and the gamma quanta produced by annihilation were registered by a scintillation counter in the analog mode. The sensitivity of the counter was calibrated by a reference β^+-source, reaching $N_{trap} = 6.66\times10^3\times V_{[V]}$ positrons, where $V_{[V]}$ is the amplitude of the signal in volts. The signal amplitude from a single positron is $V_1 = 10$ mV. This determines the statistical measurement error $\Delta N_{trap}/N_{trap} = 0.1/\sqrt{V_{[V]}}$. The positron flux injected into the trap is measured by the same counter in the counting mode as the trap is opened: $\dot{N}_{e^+} = 66.6\,\dot{N}_{counts}$.

To measure the transverse dimensions of the positron bunches, mobile collector *9* and a scintillation counter were used.

In experiments with electrons, the beam is formed by a three-electrode gun with an impregnated oxide cathode, which has a diameter of 2 mm. The cathode potential is -50 eV. The length and repetition rate of voltage pulses applied to the control electrode define the time-average value of the electron flux. Such an injection regime allows imitating the process of accumulation from a radioactive source with a fixed value of the particle flux.

When working with electrons, the charge accumulated in the trap is dropped on the collector and is measured using a current amplifier that has an equivalent input resistance $R = 300$ kΩ; the pulse FWHM is 1 μs. Accordingly, $N_{trap} = 2.1\times10^7 V_{[V]}$. The transverse dimensions of the electron bunches were measured by phosphor fluorescence *9* using a CCD camera.

The effect of accumulated particle bunch compression, observed in [56, 57], was confirmed in our experiments [48, 49, 62] for positrons and electrons using the described methods. Figure 9 illustrates different stages of electron accumulation and the change in the bunch transverse size over time.

The main conclusion from these results is that the RW field compresses the bunch to some equilibrium size and holds it for a long time. The bunch expands as the RW field is turned off. These conclusions are also confirmed by the measurement results for the dependence of the number of accumulated electrons on the accumulation time for three different RW-field operation regimes (Fig. 10): this number increases as the RW field is turned on [62].

It was also shown that the choice of the RW-field rotation direction is critical: if the field rotates in the direction of particle drift (rotation) in crossed fields (the magnetic field of the trap solenoid and the radial electric field of the bunch space charge and the trap electrodes), then the RW-field influence is maximal; it almost vanishes for the opposite direction.

Early experiments on electrons have shown that there is a particular frequency of the RW field at which its influence significantly increases: the particle lifetimes and their quantity in the bunch increase [62]. In these experiments, around 10^8 electrons could be accumulated at the resonant frequency of approximately 600 kHz (Fig. 11). The magnetic field in the trap was increased to 1300 G (which is significant) (see Section 4.3). A similar dependence can be found in [56, 57].

Fundamentally new results were obtained in investigating the 'RW spectra' in the experiments performed in 2014–2015 [63]. We studied the RF-field frequency dependence of various parameters, such as the number of particles in the bunch N_{trap}, the efficiency of particle trapping in the accumulator ε, and the particle lifetime in the trap τ. As a result, we have studied regimes of different, low and high, rates of injecting particle fluxes and found new low-frequency resonances for the RW-field frequency, which cause a significant increase in the number of accumulated particles (Fig. 12), and also 'antiresonances' at low RW-field frequencies, around several dozen Hertz, when the field rotation leads to the complete destruction of the accumulated bunches.

The efficiency of the RW-field influence strongly depends on the distribution of the trap electrode potentials. The

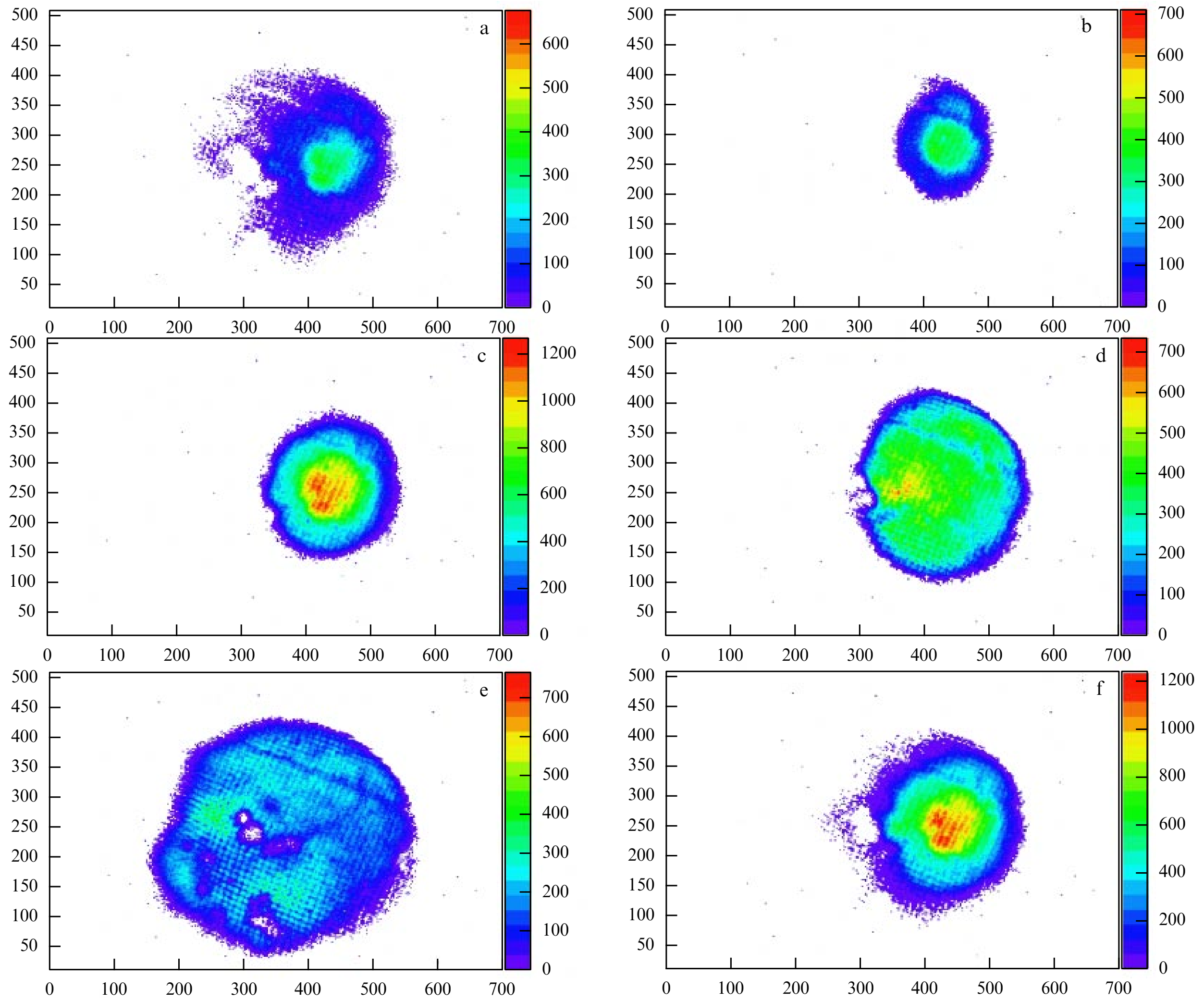

Figure 9. (Color online.) (a, b) Effect of bunch formation in the RW field after injection is stopped: the RW field is constantly operating, the injection lasts 30 s, then stops, and the resulting bunch (a) is held without injection for 30 s and (b) is sent to the phosphor. It is seen that the RW field 'removes' the halo formed during the injection. (c, d) The effect of disabling the RW field. (c) The RW field is turned on and the injection lasts 30 s. (d) After the injection stops, the bunch is held for 10 s with the RW field turned off. An expansion of the bunch is clearly seen in panel (d). (e, f) The effect of turning the RW field on and off after the injection is stopped. In both cases, the injection lasts 30 s without the RW field; after that, the injection stops and the accumulated particles are held in the trap for 10 s with the RW field being (e) turned on and (f) turned off. It can be seen from panel (f) that the RW field compresses the bunch. Photographs of the transverse cross section of the electron bunch dropped on the phosphor are made with a CCD camera. One scale division corresponds to 60 μm. The color bars on the right-hand part of the panels are the scales for the relative brightness of the image.

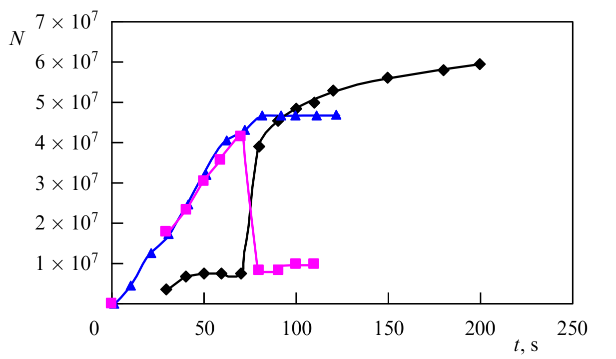

Figure 10. The number of accumulated electrons dropped on the collector $N(t)$ versus the accumulation time t for various regimes of RW-field operation: the RW field and injection turned off after 80 s, the beam freely expands (squares); the RW field is turned on after 80 s from the accumulation start (diamonds); the RW field is turned on permanently (triangles).

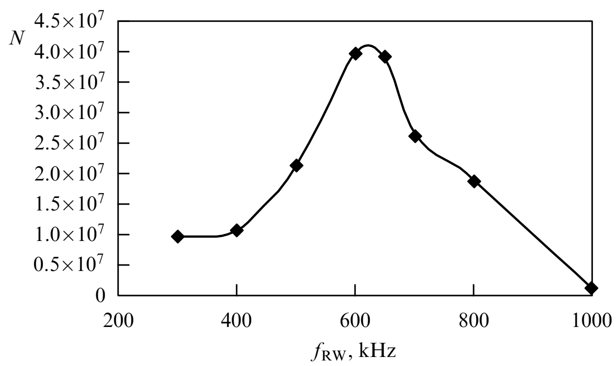

Figure 11. Dependence of the number of accumulated particles (electrons) in the bunch on the RW-field frequency for optimal parameters: $P = 2 \times 10^{-6}$ Torr, $B = 1200$ G, and $N_{e^+} \sim 10^8$.

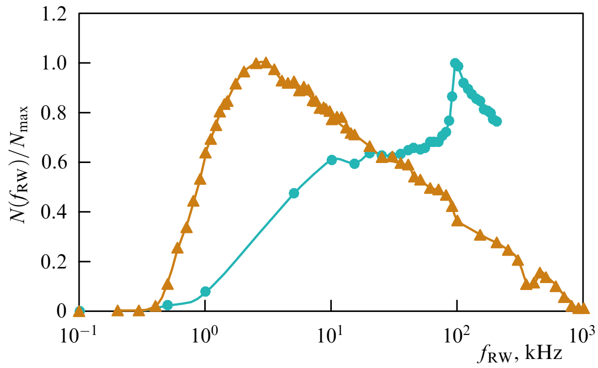

Figure 12. The number of accumulated positrons (triangles) and electrons (circles) normalized to the maximum value versus the RW-field frequency f_{RW}. The field amplitude is 1V, the buffer gas pressure in the accumulation region is 2.75×10^{-6} Torr.

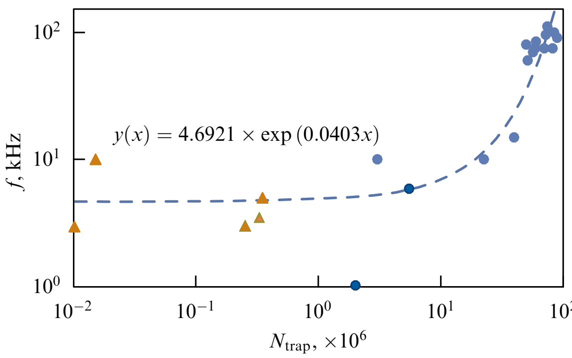

Figure 13. Dependence of the resonant frequency on the number of particles N_{trap} accumulated after 20 s: circles correspond to electrons, triangles to positrons. The dashed line is the trend $y(x) = 4.6921 \exp(0.0403x)$.

resonant frequency increases exponentially as the number of particles in the bunch N_{trap} increases (Fig. 13), and the accumulation efficiency at the resonant frequency increases as the particles accumulate, reaches its maximum, and then slightly decreases.

As the particles continuously accumulate, the change in their number in the bunch is described by

$$N_{trap}(t) = \varepsilon \dot{N} \tau \left[1 - \exp\left(-\frac{t}{\tau}\right)\right] \to \begin{cases} \varepsilon \dot{N} t, & t \ll \tau, \\ \varepsilon \dot{N} \tau, & t \gg \tau, \end{cases} \qquad (5)$$

where the trapping efficiency ε, the injecting positron flux $\dot{N}$, and the lifetime of bunch particles in the trap τ are time-independent. If the value of the flux is known, the first asymptotic form allows finding the efficiency ε, while the second one allows determining the value of $\varepsilon\tau$. Moreover,

Table 3. Dependence of the positron accumulation parameters on the buffer gas pressure P for the RW-field being turned off and on.

P, 10^{-6} Torr	τ, s RW off/RW on	ε, % RW off/RW on	$\varepsilon \times \tau$, % s RW off/RW on	N_{trap}, 10^5 RW off/RW on
1.1	4.5/12.5	1.5/1.4	6.75/17.5	0.3/0.7
4.0	5.0/8.5	6.5/7.1	32.5/60.3	1.2/2.2
7.0	5.0/9.0	11.5/11.3	57.5/101.7	1.7/2.9
10.1	5.0/7.5	16.3/17.2	81.5/129.0	2.0/3.3
13.7	3.5/6.0	25.6/23	89.6/138.0	2.1/3.2

fitting the experimental accumulation curve to relation (5) independently gives the value of τ.

In 2014–2015, we investigated the dependence of the positron accumulation efficiency on the buffer gas pressure in detail (Table 3). It can be seen from Table 3 that as the pressure is increased, the particle lifetime τ slowly decreases and the trapping efficiency ε increases. At the same time, the product $\varepsilon\tau$ also increases. Turning on the RW field at the resonant frequency almost doubles the number of accumulated positrons. The obtained experimental data were used to formulate the model for the particle accumulation mechanism in the PMS trap.

4.3 Three-dimensional model of charge motion in a trap. Mechanism of bunch compression and the increase in particle lifetimes

The effect of RW-field influence on the transverse size of the bunch still has no clear explanation [60, 61]. The authors of [64] tried to use the theory of electromechanical or electrostatic waves in a cylindrical plasma column [65, 66]. According to this theory, the plasma column has Gould–Trivelpiece vibrational modes. Being in resonance with these modes, the RW field excites the charged plasma column, but the reason for the bunch compression is not clear.

However, in the next experiments, the compressive influence of the RW field was observed in the cases of extremely small concentrations of accumulated particles, when it is impossible to excite plasma waves [60, 61]. Obviously, in the case of a small number of particles, the focusing effect should follow from the solution of the equations of motion for a single particle in the force fields that act in the trap. Such an attempt was made in [61], but the obtained solution does not give clear physical justification for the effect. Previously, experiments [57] showed a good match between the frequency and the rotation direction of the RW field with the frequency and the direction of the macroscopic drift of the whole bunch in crossed magnetic and space-charge fields. Moreover, it was discovered in our paper [62] that the RW-field frequency matches the longitudinal bounce-oscillations frequency with good accuracy:

$$f_{RW}^{res} = f_{bounce} = \frac{\omega_{bounce}}{2\pi} \approx \frac{v_{||}}{2L_0}\,.$$

Here, $v_{||}$ is the longitudinal velocity of particles with respect to the axis. This was the motivation to perform a 3D analysis of particle dynamics in the accumulation region of the trap. However, the experimental results obtained in 2014–2015 [63] forced us to reconsider this quite obvious condition. In the low-intensity range $f_{RW}^{res} \ll f_{bounce}$ (see Fig. 13), this condition is clearly not fulfilled. Therefore, we have reconsidered the particle motion analysis in the trap with the RW field.

Equations for particle motion in a homogeneous magnetic field $\mathbf{B}$ and $\mathbf{E}_{RW}$ have the well-known form

$$m\,\frac{d^2x}{dt^2} = e\,\frac{dy}{dt}\,\frac{B}{c} + e\big[E_x + E_{RW}\cos(\omega_{RW}t + \varphi)\big] - K\,\frac{dx}{dt}\,,$$
$$m\,\frac{d^2y}{dt^2} = -e\,\frac{dx}{dt}\,\frac{B}{c} + e\big[E_y + E_{RW}\sin(\omega_{RW}t + \varphi)\big] - K\,\frac{dy}{dt}\,. \qquad (6)$$

Here, m and e are the mass and charge of the particle, x and y are its coordinates in the plane perpendicular to the trap axis, $\mathbf{E} = \{E_x, E_y, E_z\}$ is the field of the trap electrodes and space charge of the bunch, and K is the friction coefficient, which takes the influence of elastic collisions with the buffer gas molecules into account. Neglecting the influence of the field **E** [it is negligible inside electrode *4* (Fig. 8a)] and the buffer gas (discussed below) in (6) and introducing the complex variable $\xi = x + \mathrm{i}y$, we transform the system of equations into

$$\frac{\mathrm{d}^2\xi}{\mathrm{d}x^2} + \omega_{\mathrm{c}}\,\frac{\mathrm{d}\xi}{\mathrm{d}t} = \frac{eE_{\mathrm{RW}}}{m}\,\exp\left[\mathrm{i}(\omega_{\mathrm{RW}}t + \varphi)\right],$$

where $\omega_{\mathrm{c}} = eB/(mc)$ is the cyclotron frequency. In the approximation $\omega_{\mathrm{c}} \gg \omega_{\mathrm{RW}}$ ('magnetized' particle), we can limit ourselves to the consideration of a particular solution:

$$\begin{aligned} x(t) &= x_0 + \frac{v_{\mathrm{d}}}{\omega_{\mathrm{RW}}}\left[\cos(\omega_{\mathrm{RW}}t + \varphi) - \cos\varphi\right], \\ y(t) &= \operatorname{Im}\xi(t) = y_0 + \frac{v_{\mathrm{d}}}{\omega_{\mathrm{RW}}}\left[-\sin(\omega_{\mathrm{RW}}t + \varphi) + \sin\varphi\right], \\ v_{\mathrm{d}} &= c\,\frac{E_{\mathrm{RW}}}{B}\,. \end{aligned} \tag{7}$$

Here, (x_0, y_0) are the coordinates of the initial position of the particle, φ is the RW-field phase at the initial instant $t = 0$, and v_{d} is the particle drift velocity in the crossed fields $\mathbf{E}_{\mathrm{RW}} \times \mathbf{B}$. Particle trajectory (7) is described by the equation of a circle

$$\left(x - x_0 + \frac{v_{\mathrm{d}}}{\omega_{\mathrm{RW}}}\cos\varphi\right)^2 + \left(y - y_0 + \frac{v_{\mathrm{d}}}{\omega_{\mathrm{RW}}}\sin\varphi\right)^2 = \left(\frac{v_{\mathrm{d}}}{\omega_{\mathrm{RW}}}\right)^2 \tag{8}$$

with the radius

$$\rho_{\mathrm{RW}} = \frac{v_{\mathrm{d}}}{\omega_{\mathrm{RW}}} = \frac{cE_{\mathrm{RW}}}{B\omega_{\mathrm{RW}}} \tag{9}$$

and center at the point $(x_0 - \rho_{\mathrm{RW}}\cos\varphi,\ y_0 - \rho_{\mathrm{RW}}\sin\varphi)$ (Fig. 14). This simplified consideration that does not take the spatial variation of $\mathbf{E}_{\mathrm{RW}}$ into account allows understanding the character of the particle motion in the PMS trap.

The trajectory of a particle in the transverse plane outside the RW field is a superposition of fast cyclotron rotation ω_{c} and a slow magnetron turn with respect to the symmetry axis of a radial electric field. The friction that occurs during collisions leads to the squeezing of the cyclotron rotation orbits and unwinds the magnetron motion trajectory: the accumulated particles diffuse on the vacuum chamber walls and disappear. A buffer gas, as was mentioned in Section 4.1,

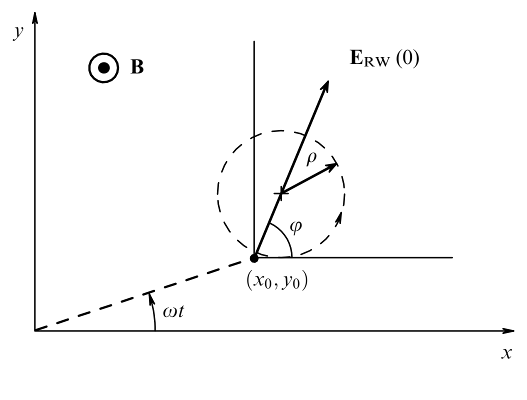

Figure 14. Trajectory of a particle in homogeneous crossed fields: the magnetic field **B** and the rotating field $\mathbf{E}_{\mathrm{RW}}$. The arrow at the particle trajectory (dashed circle) indicates the rotation direction.

is needed for the trapping of particles in the accumulation region, but its influence significantly decreases the particle lifetime. The RW field in electrode *4* (Fig. 8, a) is conservative, and (which may seem paradoxical) it can decrease the size of the bunch, increase the particle lifetime, and subsequently enhance the accumulation efficiency. This effect takes place if the RW-field frequency is adjusted to the frequencies ω_{magn} of the magnetron rotation and longitudinal oscillations of the particles. Otherwise, the average action of the RW field is zero. If a particle enters the region with the RW field at a point $(x_0,\ y_0)$, it starts to move along a circular trajectory with radius (9), and φ is the angle between the vector $\mathbf{E}_{\mathrm{RW}}$ and the x axis at the initial instant (see Fig. 14).

After interacting with the RW field for the time τ_{RW}, the particle covers the segment of the circle $\Delta s = R_{\mathrm{RW}}\omega_{\mathrm{RW}}\tau_{\mathrm{RW}}$ towards the trap axis if the angle ϕ has the optimal value at the initial instant. The rotation frequency (angular velocity of the particle) equals the RW-field frequency ω_{RW}. After leaving the region with the RW field, the particle rotates around the trap axis in crossed fields — the radial electric field of the electrodes and the accumulated particle bunch, and the magnetic field of the trap. If the particle returns to the initial point after the period of bounce-oscillations, it continues its motion along circular orbit (8) under the action of the RW field.

The radial motion (drift) of the particles under the action of the RW field must stop in the axial region of the trap, for accumulation to occur. There are several reasons for this in the PMS trap. The main one is the decrease in the particle energy after collisions with the buffer gas and thermalization of the gas–particles system to room temperature. As a result, the depth of the particle penetration inside the RW-field region gradually decreases with time (see the plot of the function $U(z)$ in Fig. 8b). The RW field rapidly decreases near the edges of electrodes *4* and *5*; therefore, the radius $\rho_{\mathrm{RW}}(z)$ of the circular trajectory in Eqn (9) decreases. Figure 15 shows a special case of such a trajectory. The process ends with a 'stop' of the particle near the trap axis.

The process ends with the formation of a particle bunch in an axial region of the trap potential well [inside electrodes *5* and *6* (Fig. 8a)]. The competing process — diffusion through collisions with the buffer gas — is compensated by the action of the RW field.

This accumulation scheme is confirmed by the dependences of ε and τ on the buffer gas pressure (see Table 3).

The 3D-resonance condition follows from the proposed accumulation scheme. After the period of particle longitudinal oscillations T_{bounce}, the RW-field vector rotates through the angle $\Delta\varphi_{\mathrm{RW}} = \omega_{\mathrm{RW}}T_{\mathrm{bounce}}$ and the particle shifts along the azimuth with respect to the trap axis by an angle of magnetron rotation:

$$\Delta\varphi_{\mathrm{e}} = \int_0^{T_{\mathrm{bounce}}} \omega_{\mathrm{magn}}(t)\,\mathrm{d}t + \omega_{\mathrm{RW}}\tau_{\mathrm{RW}}\,, \tag{10}$$

where τ_{RW} is the time of particle interaction with the RW field. The relations $\Delta\varphi_{\mathrm{RW}} = \Delta\varphi_{\mathrm{e}} + 2\pi n$ and (10) determine the resonance condition

$$(\omega_{\mathrm{RW}})_{\mathrm{res}} = \frac{\int_0^{T_{\mathrm{bounce}}} \omega_{\mathrm{magn}}(t)\,\mathrm{d}t + 2\pi n}{T_{\mathrm{bounce}} - \tau_{\mathrm{RW}}}\,. \tag{11}$$

Relation (11) is approximate. It holds for

$$\Delta s \ll R_{\mathrm{RW}}\,, \quad \text{or} \quad \omega_{\mathrm{RW}}\tau_{\mathrm{RW}} \ll 1\,. \tag{12}$$

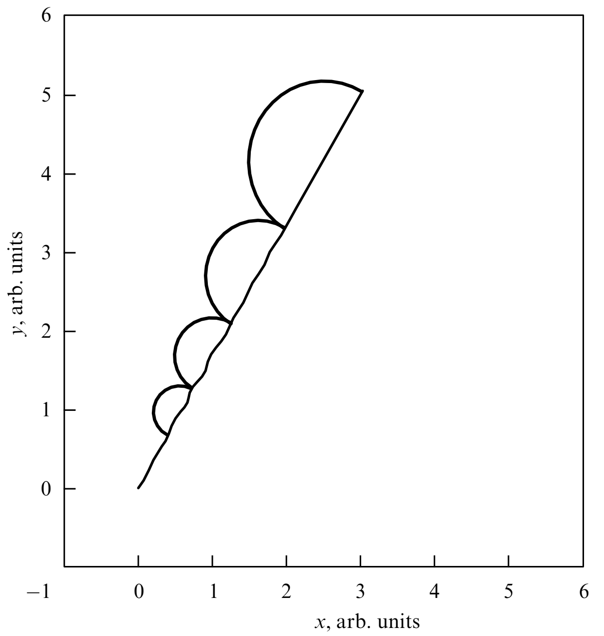

Figure 15. Particle trajectory in the RW-field region after multiple bounce-oscillations. The trap axis is located at $x = y = 0$, $\phi = 59°$, $(R_{\rm RW})_n = k^{n-1}(R_{\rm RW})_1$, $k = 0.7$, $n = 1, 2, \ldots$, $(R_{\rm RW})_1 = 1.0$; the frequency $\omega_{\rm RW}$ is chosen such that the particle experiences a half-turn in the RW-field region.

We note that $T_{\rm bounce}$ and $\tau_{\rm RW}$ depend on the particle energy; therefore, $(\omega_{\rm RW})_{\rm res}$ depends on it as well. As a result, the RW spectrum contains information about the energy spectrum of particles in the trap, and each frequency is 'resonant' for particles with a specific energy.

If the intensity of the accumulated bunches is low, the magnetron motion period is determined by the particle rotation in the transverse electric field of trap electrodes close to the points of turning in electrodes *4*, *7*, *8* (Fig. 8a). For larger intensities, the greatest role is played by the azimuthal drift in the crossed fields: the electric field of the space charge of the bunch and the longitudinal magnetic field. The existence of 'antiresonances' — dips in the RW spectra in low-frequency ranges of the RW field (see Fig. 12) — does not conflict with the 3D model: transverse drift in the crossed quasistatic RW field and constant magnetic field brings the particles to the vacuum chamber walls.

The above considerations show that the trapping efficiency ε has to vary during the accumulation. At the beginning, when there is a small number of particles in the bunch, the frequencies $\omega_{\rm magn}$ and $(\omega_{\rm RW})_{\rm res}$ are also small, as if the RW field were almost completely absent. As the accumulation process continues, ε increases and saturates (exactly what we see in the experiment). This brings us to the investigation of the accumulation regime with the scan over the RW-field frequency: the frequency should increase while the particles are accumulating. Such an experiment is planned to be performed soon in the PMS trap at the LEPTA setup.

Numerical simulation of particle motion in the fields of the accumulation region (Fig. 8b) has shown that the instantaneous values of the magnetron rotation frequency are maximal near the turning points inside electrodes *4*, *7*, and *8* (Fig. 8a). The longitudinal bounce-oscillation period depends on the particle energy and the distribution of the potentials in the trap and varies from several microseconds to several hundred microseconds. The time during which the accumulated particles interact with the rotating field can almost reach the bounce-oscillation period if the particles are localized in the accumulation region. This time shortens as the particle energy increases. An estimate for $\omega_{\rm RW}^{\rm res}$ from Eqn (11) for a low-intensity bunch in the PMS trap of the LEPTA setup results in a value of several kHz, which agrees with the experimental data (see Fig. 13). To provide a systematic action of the RW field on the process of accumulation and confinement of the bunch near the trap axis for larger concentrations of accumulated particles, the rotating field frequency should be proportionally increased in accordance with the relation for the magnetron rotation frequency of the bunch in the field of a space charge $\omega_{\rm RW}^{\rm res} \approx \omega_{\rm magn} = 2\pi nec/B$, where n is the concentration of particles in the bunch.

To summarize, the main properties of the 3D resonance can be formulated as follows:

(1) The angular velocity of the 'magnetized' particle on the circular orbit in the RW field is independent of the particle energy.

(2) The radius of the trajectory (circle) of the 'magnetized' particle in the RW field is proportional to the field strength $E_{\rm RW}$.

(3) The period of longitudinal oscillations depends weakly on the particle energy (a quasiparabolic potential $U(z)$ of the field created by trap electrodes).

(4) During their motion in the trap, the particles exhibit rotation around its axis under the action of crossed fields: the longitudinal magnetic field and the radial component of the electric field of the trap electrodes and the space charge of the accumulated particle bunch.

(5) A 3D resonance occurs if conditions (11) and (12) are satisfied.

5. Limit capabilities of traps and particle accumulators

There are several limitations on the number of particles that can be accumulated in a trap. The first is the limitation of the space charge. The potential formed on the axis of the chamber relative to its wall by an axially symmetric bunch of particles with the charge e and a constant concentration n is described (in the Gaussian system of units) by the known relation

$$\varphi(0) = en\pi a^2\left(2\ln\frac{b}{a} + 1\right),$$

where a and b are the radii of the particle bunch and the vacuum chamber. If $\varphi(0)$ exceeds the trapping potential ΔU, the accumulation stops. This means that the number of particles in the trap is bounded by the value

$$N_{\rm bunch} \leqslant \frac{\Delta UL}{e}\left(\frac{2\ln b}{a} + 1\right)^{-1}, \tag{13}$$

where L is the bunch length. In the case of a PMS trap in the LEPTA facility (Fig. 8a), for $a \approx 0.5$ cm, $b = 10$ cm, and $\Delta U = 13$ V, estimate (13) results in $N \approx 3 \times 10^8$ positrons.

The second limitation is also related to the Coulomb field of the bunch space charge. When the particle density reaches some critical value, the Coulomb repulsive force exceeds the Lorentz force of the magnetic field, which prevents the expansion of the bunch. The corresponding limitation is the Brillouin criterion [67]

$$n_{\mathrm{B}} \leqslant \frac{B^2}{8\pi mc^2}\,. \tag{14}$$

In the case of light-particle accumulation, this is a quite weak limitation. For example, a field of 1 kG can hold positron (electron) bunches with densities reaching 10^{11} cm^{-3}. For heavy particles (ions), the limit density decreases by 1836 A_{ion} times, where A_{ion} is the ion atomic number.

The clear advantage of the PMS magnetic trap is the simplicity of particle injection into the trap and the removal from it. This makes these traps attractive for the accumulation of charged antiparticles. However, in order to effectively capture them from the flux of a radioactive source, the buffer gas technique described above must be used. In fact, this was the suggestion made by Dehmelt [27] and developed by Surko [54] in the PMS trap. This method of injection and trapping of particles allows their accumulation from a continuous source.

For the Paul, Penning, and Penning–Malmberg traps of a conventional design, the only effective method for particle trapping is pulsed injection, when the trapping potential of one of the end electrodes is disabled, while the first particle travels from the trap entrance to the other end of the electrode and back. This limits the number of particles that can be confined in the trap.

An important advantage of Penning–Malmberg traps is their ability to hold a large number of particles due to the large longitudinal size. In the absence of scattering and diffusion on the residual gas, the particle bunch with the density that satisfies conditions (13) and (14) does not contact with the vacuum chamber walls for an arbitrarily long time. But the scattering on the molecules of the residual and buffer gas (if it is used) leads to the transverse diffusion of the particles and, consequently, to a decrease in the maximal number of accumulated charged particles. Therefore, the pressure in the vacuum chamber is limited by several microtorrs.

The lifetime of particles in traps, as is known from plasma physics and is confirmed experimentally (see, e.g., [68]), is directly proportional to the magnetic field strength and is inversely proportional to the temperature and residual gas pressure. In the case of antiparticles, there is also the effect of annihilation via collisions, and therefore the initial vacuum (before the buffer gas is supplied) should be extremely high. Another limitation for the lifetime is the scattering on unavoidable inhomogeneities of the magnetic and electric fields, which is especially highly pronounced in ring traps/accumulators [50]. The role of diffusion on the walls in this case significantly increases as the bunch length L is increased: for a high vacuum, the lifetime is proportional to $(B/L)^2$ [51].

There is also the method of charge-exchange injection, which was suggested for accelerating technologies [69]. But this method can be applied only to ions and protons. A variation of this method is the injection of particles that are produced during the decay of other particles, as is done, for example, in g-2 experiments on the measurement of the anomalous muon magnetic moment in traps/storage rings, which have been conducted at CERN and were continued at the Brookhaven National Laboratory and the Fermi National Accelerator Laboratory (USA) [70]. These experiments use a storage ring with a highly homogeneous transverse magnetic field and a focusing system of electrostatic quadrupole lenses. This provides stability of the spin dynamics of muons produced in π-meson decays.

6. Conclusion

The charged particle traps presented in this review find quite broad and diverse applications in physical experiments, each type of trap in its own field — particle, nuclear, atomic, and molecular physics. Every type of trap has its own features and limitations, advantages and disadvantages.

The most detailed description is given for the experimental results on electron and positron accumulation in the Penning–Malmberg–Surko trap with a rotating electric field. The proposed mechanism for the resonant action of this field — the 3D resonance [63] that compresses the accumulated particle bunch, increases the particle lifetime in the trap, and increases the number of accumulated particles — agrees with the experimental data. We have also formulated criteria that allow estimating the maximal number of particles that can be accumulated in a PMS trap.

The development and improvement of particle accumulation methods allow us to advance in performing new-generation experimental investigations.

Acknowledgments
The authors sincerely thank A G Kobets, O S Orlov, and A A Sidorin for taking part in joint experiments on the LEPTA facility, E V Akhmanova for numerical simulation of the accumulator fields, O I Meshkov for the valuable comments on the manuscript, G V Trubnikov and S L Yakovenko for the support and interest in the work, and L V Soboleva and T A Stepanova for help in preparing the manuscript.

References

1. Baur G et al. *Phys. Lett. B* **368** 251 (1996)
2. Andresen G B et al. (The ALPHA Collab.) *Nature Phys.* **7** 558 (2011)
3. Amole C et al. *Nature* **483** 439 (2012)
4. Kuroda N et al. *Nature Commun.* **5** 3089 (2014)
5. Pérez P et al. *Hyperfine Interact.* **233** 21 (2015)
6. Scampoli P, Storey J *Mod. Phys. Lett. A* **29** 143001 (2014)
7. Bertsche W A et al. *J. Phys. B* **48** 232001 (2015)
8. Meshkov I N *Phys. Part. Nucl.* **28** 198 (1997); *Fiz. Elem. Chastits At. Yadra* **28** 495 (1997)
9. Danielson J R et al. *Rev. Mod. Phys.* **87** 247 (2015)
10. Gribakin G F, Young J A, Surko C M *Rev. Mod. Phys.* **82** 2557 (2010)
11. Cassidy D B, Mills A P (Jr.) *Nature* **449** 195 (2007)
12. Cassidy D B et al. *Phys. Rev. Lett.* **108** 043401 (2012)
13. Cassidy D B et al. *Phys. Rev. Lett.* **108** 133402 (2012)
14. Major F G, Gheorghe V N, Werth G *Charged Particle Traps. Physics and Techniques of Charged Particle Field Confinement* (Berlin: Springer, 2005)
15. Werth G, Gheorghe V N, Major F G *Charged Particle Traps II: Applications* (Berlin: Springer, 2009)
16. Kadomtsev B B, in *Fizicheskaya Entsiklopediya* (Physical Encyclopedia) Vol. 5 (Ed.-in-Chief A M Prokhorov) (Moscow: Bol'shaya Rossiiskaya Entsiklopediya, 1998) p. 119
17. Spitzer L (Jr.) *Sci. Am.* **199** (4) 28 (1958); Translated into Russian: *Usp. Fiz. Nauk* **71** 327 (1960)
18. Budker G I, in *Plasma Physics and the Problem of Controlled Thermonuclear Reactions* Vol. 3 (Ed. M A Leontovich) (New York: Pergamon Press, 1959) p. 1; Translated from Russian: *Fizika Plazmy i Problema Upravlyaemykh Termoyadernykh Reaktsii* Vol. 3 (Ed. M A Leontovich) (Moscow: Izd. AN SSSR, 1958) p. 3
19. Post R F *Rev. Mod. Phys.* **28** 338 (1956)

20. Pierce J R *Theory and Design of Electron Beams* (New York: Van Nostrand Co., 1949)
21. Dehmelt H *Adv. At. Mol. Phys.* **3** 53 (1967)
22. Dehmelt H *Adv. At. Mol. Phys.* **5** 109 (1969)
23. Wineland D, Ekstrom P, Dehmelt H *Phys. Rev. Lett.* **31** 1279 (1973)
24. Penning F M *Physica* **3** 873 (1936)
25. Paul W, Steinwedel H *Z. Naturforsch. A* **8** 448 (1953)
26. Paul W *Rev. Mod. Phys.* **62** 531 (1990); *Usp. Fiz. Nauk* **160** (12) 109 (1990)
27. Dehmelt H *Rev. Mod. Phys.* **62** 525 (1990); *Usp. Fiz. Nauk* **160** (12) 129 (1990)
28. Meshkov I N, in *Fizicheskaya Entsiklopediya* Vol. 1 (Ed.-in-Chief A M Prokhorov) (Moscow: Sovetskaya Entsiklopediya, 1988) p. 351
29. Vladimirskii V V *Sov. Phys. JETP* **12** 740 (1961); *Zh. Eksp. Teor. Fiz.* **39** 1062 (1960)
30. Gott Yu V, Ioffe M S, Tel'novsky V G, in *Nuclear Fusion Supplement* Vol. 3 (Vienna: International Atomic Energy Agency, 1962) p. 1045
31. Pritchard D E *Phys. Rev. Lett.* **51** 1336 (1983)
32. Toschek P E, in *Tendances Actuelles en Physique Atomique. New Trends in Atomic Physics. Les Houches, Session XXXVIII, June 28 – July 29, 1982* Vol. 1 (Eds G Grynberg, R Stora) (Amsterdam: North-Holland, 1984) p. 383; Translated into Russian: *Usp. Fiz. Nauk* **158** 451 (1989)
33. Minogin V G *Sov. Phys. Usp.* **25** 359 (1982); *Usp. Fiz. Nauk* **137** 173 (1982)
34. Chu S *Rev. Mod. Phys.* **70** 685 (1998); *Usp. Fiz. Nauk* **169** 274 (1999)
35. Ketterle W *Rev. Mod. Phys.* **74** 1131 (2002); *Usp. Fiz. Nauk* **173** 1339 (2003)
36. Wineland D J *Rev. Mod. Phys.* **85** 1103 (2013); *Usp. Fiz. Nauk* **184** 1089 (2014)
37. Dehmelt H G, Schwinberg P B, Van Dyck R S *Int. J. Mass Spectrom. Ion Phys.* **26** 107 (1978)
38. Schwinberg P B, Van Dyck R S (Jr.), Dehmelt H G *Phys. Lett. A* **81** 119 (1981)
39. Tarantin N I *Phys. Part. Nucl.* **30** 167 (1999); *Fiz. Elem. Chastits At. Yadra* **30** 402 (1999)
40. Marrs R E, Elliott S R, Knapp D A *Phys. Rev. Lett.* **72** 4082 (1994)
41. Jonson B *Phys. Rep.* **389** 1 (2004)
42. Chen L et al. *Nucl. Phys. A* **882** 71 (2012)
43. Schneider Ch, Porras D, Schaetz T *Rep. Prog. Phys.* **75** 024401 (2012)
44. Malmberg J H, Driscoll C F *Phys. Rev. Lett.* **44** 654 (1980)
45. Benilan M-N, Audoin C *Int. J. Mass Spectrom. Ion Phys.* **11** 421 (1973)
46. Gabrielse G, Mackintosh F C *Int. J. Mass Spectrom. Ion Proces.* **57** 1 (1984)
47. Meshkov I, Skrinsky A *Nucl. Instrum. Meth. Phys. Res. A* **379** 41 (1996); Preprint E9-95-130 (Dubna: JINR, 1995)
48. Akhmanova E V et al. *Phys. Part. Nucl. Lett.* **7** 502 (2010); *Pis'ma Fiz. Elem. Chastits At. Yadra* **7** 814 (2010)
49. Akhmanova E V et al. *Phys. Part. Nucl. Lett.* **9** 373 (2012); *Pis'ma Fiz. Elem. Chastits At. Yadra* **9** 618 (2012)
50. Meshkov I N et al. *Phys. Part. Nucl.* **36** 562 (2005); *Fiz. Elem. Chastits At. Yadra* **36** 1071 (2005)
51. Eseev M K *Ekzoticheskie Atomy, Iony i Ikh Komponenty v Intensivnykh Elektromagnitnykh Polyakh* (Exotic Atoms, Ions and Their Components in Intensive Electromagnetic Fields) (Arkhangel'sk: SAFU, 2014)
52. Meshkov I N *Phys. Part. Nucl.* **28** 198 (1997); *Fiz. Elem. Chastits At. Yadra* **28** 495 (1997)
53. Meshkov I N *AIP Conf. Proc.* **592** 616 (2001)
54. Surko C M, Leventhal M, Passner A *Phys. Rev. Lett.* **62** 901 (1989)
55. Huang X-P et al. *Phys. Rev. Lett.* **78** 875 (1997)
56. Greaves R G, Surko C M *Phys. Rev. Lett.* **85** 1883 (2000)
57. Danielson J R, Surko C M *Phys. Plasmas* **13** 055706 (2006)
58. Andresen G B et al. (ALPHA Collab.) *Phys. Rev. Lett.* **100** 203401 (2008)
59. Danielson J R et al. *Phys. Rev. Lett.* **109** 113201 (2012)
60. Greaves R G, Moxom J M *Phys. Plasmas* **15** 072304 (2008)
61. Isaac C A et al. *Phys. Rev. Lett.* **107** 033201 (2011)
62. Eseev M K et al. *Plasma Phys. Rep.* **39** 787 (2013); *Fiz. Plazmy* **39** 883 (2013)
63. Eseev M K et al. *JETP Lett.* **102** 261 (2015); *Pis'ma Zh. Eksp. Teor. Fiz.* **102** 291 (2015)
64. Danielson J R, Surko C M, O'Neil T M *Phys. Rev. Lett.* **99** 135005 (2007)
65. Trivelpiece W, Gould R W *J. Appl. Phys.* **30** 1784 (1959)
66. Anderegg F, Hollmann E M, Driscoll C F *Phys. Rev. Lett.* **81** 4875 (1998)
67. Brillouin L *Phys. Rev.* **67** 260 (1945)
68. Luk'yanov S Yu *Goryachaya Plazma i Upravlyaemyi Yadernyi Sintez* (Hot Plasma and Controlled Nuclear Synthesis) (Moscow: Nauka, 1975)
69. Budker G I, Dimov G I, Dudnikov V G *Sov. Atom. Energy* **22** 441 (1967); *Atom. Energ.* **22** 348 (1967)
70. Bennett G W et al. (Muon (g-2) Collab.) *Phys. Rev. Lett.* **92** 161802 (2004)